

Sequential Parametric Optimization for Rate-Splitting Precoding in Non-Orthogonal Unicast and Multicast Transmissions

Luis F. Abanto-Leon[†], Matthias Hollick[†], Bruno Clerckx[‡], Gek Hong (Allyson) Sim[†],

[†]Secure Mobile Networking (SEEMOO) Lab, Technical University of Darmstadt, Germany

[‡]Imperial College London, United Kingdom

Email: [†]{labanto,asim,mhollick}@seemoo.tu-darmstadt.de, [‡]b.clerckx@imperial.ac.uk

Abstract—This paper investigates rate-splitting (RS) precoding for non-orthogonal unicast and multicast (NOUM) transmissions using fully-digital and hybrid precoders. We study the nonconvex weighted sum-rate (WSR) maximization problem subject to a multicast requirement. We propose FALCON, an approach based on sequential parametric optimization, to solve the aforementioned problem. We show that FALCON converges to a local optimum without requiring judicious selection of an initial feasible point. Besides, we show through simulations that by leveraging RS, hybrid precoders can attain nearly the same performance as their fully-digital counterparts under certain specific settings.

Index Terms—parametric optimization, SDP, unicast, multicast, non-orthogonal multiple access, rate-splitting.

I. INTRODUCTION

The upsurge of wireless applications and the increasing omnipresence of internet-of-things (IoT) devices are expected to exacerbate the scarcity of radio resources. Moreover, recent requirements to support multiple services simultaneously (e.g., concurrent unicast and multicast) will further aggravate the situation. This state of affairs has invigorated research on non-orthogonal unicast and multicast (NOUM) transmissions and millimeter-wave. On the one hand, NOUM has been envisaged as a recourse for improving spectral efficiency due to its capability of providing concurrent services in the same radio frequency resources. Specifically, NOUM has encountered outstanding solutions through layered-division-multiplexing (LDM) [1] and rate-splitting (RS) [2]. On the other hand, usage of the underexploited millimeter-wave spectrum is a promising solution to alleviate the scarcity of radio resources. However, the adoption of (traditional) fully-digital precoders at high frequencies is challenging owing to prohibitive fabrication costs and excessive power consumption. Consequently, the more power-efficient hybrid precoders have emerged as a functional solution to overcome such difficulties.

Motivation: Inspired by the exceptional spectral efficiency achieved by fully-digital precoders in RS-NOUM [2], [3], and the predominant use of hybrid precoders in millimeter-wave communications, we investigate the weighted sum-rate (WSR) maximization problem with both fully-digital and hybrid precoders in millimeter-wave RS-NOUM systems. Further, the body of work on WSR maximization with RS precoding leverages weighted minimum mean square error (WMMSE) [2], [4]–[6] as a prevailing means of solution. In this paper, we propose FALCON, which is based on sequential parametric optimization and compared to WMMSE. Our contributions are:

- We propose FALCON, a fast convergence algorithm for solving the nonconvex WSR maximization problem. Our approach leverages semidefinite programming (SDP) and successive convex approximations (SCA). Specifically, we exploit sub-level/super-level sets and establish parametric convex upper bounds that can be contracted iteratively [7]. We show that FALCON converges to a local optimum of the nonconvex WSR maximization problem. Further, FALCON does not rely on judicious selection of initial feasible points (as WMMSE does) in order to guarantee high performance.
- We use FALCON and WMMSE with both RS-NOUM and LDM-NOUM systems. We realize that the former outperforms the latter due to the capability of RS to partially decode interference and partially treat remaining interference as noise. We compare RS-NOUM against the optimal dirty paper coding, thus revealing a small optimality gap between the two schemes.
- We find that, under specific settings, quantizing the hybrid precoder phase shifts with 4 bits is sufficient to achieve the same performance as fully-digital implementations. Further, in scenarios wherein users have channels with a low degree of correlation, such performance can be attained with 2 bits.
- We show, through simulations, that FALCON is less prone than WMMSE to return infeasible solutions due to its non-dependency on initial feasible points. Nevertheless, FALCON has higher computational complexity per iteration.

II. RELATED WORK

NOUM has been studied under LDM in [1], [8]–[14]. Specifically, [1], [8], [9] investigate the design of fully-digital precoders for transmit power minimization with unicast and multicast quality-of-service (QoS) requirements. A fairness-aware hybrid precoder is proposed in [10], [15]. Energy efficiency with fully-digital precoders is investigated in [11], [12] whereas a similar setting with backhaul constraints is considered in [13], [14]. On the other hand, NOUM with RS has only been researched with fully-digital precoders in [2], [3], wherein the WMMSE approach is proposed for WSR maximization. Relevant literature on other aspects of RS includes [4], [5], [16]–[20]. *Although both LDM and RS are power-domain non-orthogonal schemes, the superiority of RS resides in its capability to partially decode interference. This is achieved by embedding fragments of unicast information in the multicast signal, that the receivers can decode and remove.*

III. SYSTEM MODEL: RS FOR NOUM TRANSMISSIONS

We consider a system where a next-generation Node B (gNodeB) serves K single-antenna users indexed by $\mathcal{K} = \{1, \dots, K\}$. The gNodeB is equipped with a hybrid transmitter composed of N_{tx} transmit antennas and $N_{\text{tx}}^{\text{RF}}$ radio frequency (RF) chains, where $K \leq N_{\text{tx}}^{\text{RF}} \leq N_{\text{tx}}$. Without loss of generality, we assume $N_{\text{tx}}^{\text{RF}} = K$. The gNodeB transmits in a non-orthogonal manner a multicast message $W^{(\text{m})}$ (intended to all the users) and K unicast messages $W_1^{(\text{u})}, \dots, W_K^{(\text{u})}$ (each targeting a particular user). Every unicast message is decomposed into two components as $W_k^{(\text{u})} \triangleq (W_k^{(\text{u},\text{c})}, W_k^{(\text{u},\text{p})})$, where $W_k^{(\text{u},\text{c})}$ and $W_k^{(\text{u},\text{p})}$ are referred as the common and private parts, respectively. The multicast message along with the unicast common parts are jointly encoded into a common macro-stream as $\{W_1^{(\text{u},\text{c})}, \dots, W_K^{(\text{u},\text{c})}, W^{(\text{m})}\} \mapsto \tilde{\mathbf{z}} = [\tilde{z}_1, \tilde{z}_2, \dots]^T$. The unicast private parts are encoded into independent streams as $W_k^{(\text{u},\text{p})} \mapsto \tilde{\mathbf{s}}_k = [\tilde{s}_{k,1}, \tilde{s}_{k,2}, \dots]^T, \forall k \in \mathcal{K}$. The encoded streams are processed by the baseband digital precoder $[\mathbf{B}|\mathbf{m}] = [\mathbf{b}_1, \dots, \mathbf{b}_K, \mathbf{m}] \in \mathbb{C}^{K \times (K+1)}$ of the hybrid transmitter. Let z and $\mathbf{s} = [s_1, \dots, s_K]^T$ denote the instantaneous symbol and vector symbol of the common macro-stream and private streams, respectively, such that $\mathbb{E}\{[\mathbf{s}^T|z]^H [\mathbf{s}^T|z]\} = \mathbf{I}$. Thus, the downlink signal is $\mathbf{x} = \mathbf{F}[\mathbf{B}|\mathbf{m}][\mathbf{s}^T|z]^T \in \mathbb{C}^{N_{\text{tx}} \times 1}$, where $\mathbf{F} = [\mathbf{f}_1, \dots, \mathbf{f}_K] \in \mathbb{C}^{N_{\text{tx}} \times K}$ represents the RF analog precoder of the hybrid transmitter. Under flat fading, the signal received by the k -th user is

$$y_k = \underbrace{\mathbf{h}_k^H \mathbf{F} \mathbf{m} z}_{\text{common signal } y_k^{(\text{c})}} + \underbrace{\mathbf{h}_k^H \mathbf{F} \mathbf{b}_k s_k}_{\text{private signal for user } k, y_k^{(\text{p})}} + \underbrace{\mathbf{h}_k^H \mathbf{F} \sum_{j \neq k} \mathbf{b}_j s_j}_{\text{interference at user } k, y_k^{(\text{i})}} + \underbrace{n_k}_{\text{noise}}, \quad (1)$$

where $n_k \sim \mathcal{CN}(0, \sigma^2)$ denotes additive white Gaussian noise and $\mathbf{h}_k \in \mathbb{C}^{N_{\text{tx}} \times 1}$ represents the channel between the gNodeB and the k -th user. Because the users have a single antenna, they are not capable of performing spatial demultiplexing to separate the two data streams. In order to distinguish and decode both signals, the users rely on successive interference cancellation (SIC), which consists in detecting and decoding one signal after the other, as explained in the following. First, each user k decodes the common macro-stream symbol z , in term $y_k^{(\text{c})}$, by treating the rest of signals as noise. Subsequently, the common signal $y_k^{(\text{c})}$ is reconstructed and subtracted from y_k . At this point, the remaining byproduct $\tilde{y}_k = y_k - y_k^{(\text{c})}$ consists solely of private unicast components $\{y_k^{(\text{p})}, y_k^{(\text{i})}\}$ and noise n_k , from where user k decodes symbol s_k . Thus, the signal-to-interference-plus-noise ratio (SINR) of the common macro-stream and private streams are denoted by $\text{SINR}_k^{(\text{c})}$ and $\text{SINR}_k^{(\text{p})}$, respectively.

$$\text{SINR}_k^{(\text{c})} = \frac{|\mathbf{h}_k^H \mathbf{F} \mathbf{m}|^2}{\sum_{j \in \mathcal{K}} |\mathbf{h}_k^H \mathbf{F} \mathbf{b}_j|^2 + \sigma^2} \quad \text{SINR}_k^{(\text{p})} = \frac{|\mathbf{h}_k^H \mathbf{F} \mathbf{b}_k|^2}{\sum_{j \neq k} |\mathbf{h}_k^H \mathbf{F} \mathbf{b}_j|^2 + \sigma^2}$$

RS principle: Based on the expressions above, the achievable rates are $R_k^{(\text{c})} = \log_2(1 + \text{SINR}_k^{(\text{c})})$ and $R_k^{(\text{p})} = \log_2(1 + \text{SINR}_k^{(\text{p})})$. We define $\bar{R}^{(\text{c})}$ as the maximal rate at which all users can successfully decode the common symbol z . Thus, the common macro-stream is to be encoded at a rate $\bar{R}^{(\text{c})} \leq R_{\min}^{(\text{c})}$, where $R_{\min}^{(\text{c})} = \min_{k \in \mathcal{K}} \{R_1^{(\text{c})}, \dots, R_K^{(\text{c})}\}$. Since z results from jointly encoding multiple messages, let C_0 denote

the fraction of $\bar{R}^{(\text{c})}$ conveying the multicast message $W^{(\text{m})}$, and C_k the fraction of $\bar{R}^{(\text{c})}$ transmitting the unicast common part $W_k^{(\text{u},\text{c})}$, subject to $C_0 + \sum_{k \in \mathcal{K}} C_k = \bar{R}^{(\text{c})}$. Upon decoding the streams $\tilde{\mathbf{z}}$ and $\tilde{\mathbf{s}}_k$, user k acquires $W_1^{(\text{u},\text{c})}, \dots, W_K^{(\text{u},\text{c})}, W^{(\text{m})}$ and $W_k^{(\text{u},\text{p})}$, from where the unicast message $W_k^{(\text{u})}$ can be reassembled. The common parts $W_{j \neq k}^{(\text{u},\text{c})}$ decoded by user k are used for interference decoding, thus improving the SINR. The aggregate unicast rate of user k is $R_k^{(\text{u})} = C_k + \log_2(1 + \text{SINR}_k^{(\text{p})})$.

IV. PROBLEM FORMULATION

The QoS-constrained WSR maximization problem is

$$\mathcal{P} : \max_{C_0, C_k, \mathbf{F}, \mathbf{b}_k, \mathbf{m}} \sum_{k \in \mathcal{K}} \mu_k \left(C_k + \log_2(1 + \text{SINR}_k^{(\text{p})}) \right) \quad (2a)$$

$$\text{s.t.} \quad C_0 + \sum_{j \in \mathcal{K}} C_j = \bar{R}^{(\text{c})}, \quad (2b)$$

$$C_0 \geq C_0^{\text{th}}, \quad (2c)$$

$$C_k \geq 0, \forall k \in \mathcal{K}, \quad (2d)$$

$$\|\mathbf{F} \mathbf{m}\|_2^2 + \sum_{k \in \mathcal{K}} \|\mathbf{F} \mathbf{b}_k\|_2^2 \leq P_{\text{tx}}, \quad (2e)$$

$$[\mathbf{F}]_{n_1, n_2} \in \mathcal{F}, n_1 \in \mathcal{N}_1, n_2 \in \mathcal{N}_2, \quad (2f)$$

where $\mu_k > 0$ in (2a) is the weight assigned to the k -th unicast rate and (2b) enforces the sum of *rate fractions* to be $\bar{R}^{(\text{c})}$. The constraint (2c) imposes a minimum QoS requirement C_0^{th} , necessary for decoding the multicast message whereas (2d) imposes a non-negativity restriction on the rates C_k . The constraint (2e) restricts the transmit power to P_{tx} while (2f) enforces the limitations of analog beamforming. Concretely, every phase shift $[\mathbf{F}]_{n_1, n_2}$ is constrained to the feasible set $\mathcal{F} = \left\{ \delta_{\text{tx}}, \dots, \delta_{\text{tx}} \exp\left(j \frac{2\pi(L_{\text{tx}} - 1)}{L_{\text{tx}}}\right) \right\}$, where L_{tx} is the number of allowed constant-modulus phase shifts, $\delta_{\text{tx}} = \sqrt{1/N_{\text{tx}}^{\text{RF}}}$, $n_1 \in \mathcal{N}_1 = \{1, \dots, N_{\text{tx}}\}$ and $n_2 \in \mathcal{N}_2 = \{1, \dots, N_{\text{tx}}^{\text{RF}}\}$.

A. WSR maximization using fully-digital precoders

In this case, $\mathbf{F} = \mathbf{I}$ thereby transforming the hybrid precoder into a fully-digital precoder, where the number of antennas and RF chains are the same. Note that this assumption removes the nonconvex constraint (2f). As a result, \mathcal{P} and \mathcal{Q}_2 (shown in Section IV-B) become equivalent.

B. WSR maximization using hybrid precoders

The hybrid precoder consists of a coupled architecture between an analog component \mathbf{F} and a digital component $[\mathbf{B}|\mathbf{m}]$. This structure poses a difficulty in obtaining an optimal solution for \mathcal{P} . Therefore, we design the hybrid precoder by means of two suboptimal methods that prove to have high performance when compared to the fully-digital precoder (as evidenced in Section VI). These suboptimal methods consist of two stages: in *Stage 1* we design the analog precoder whereas in *Stage 2* we optimize the rate-splitting and digital precoders.

Stage 1 (Analog precoder design): To design the RF analog precoder $\mathbf{F} = [\mathbf{f}_1, \dots, \mathbf{f}_K]$, two methods are devised with the goal of maximizing the effective RF-to-RF channel gain of every user. Notice that \mathbf{F} is optimized only once as it is matched to the channels $\{\mathbf{h}_k\}_{k=1}^K$, which are deemed invariant for a number of channel uses.

Codebook-based (CB): This method designs \mathbf{F} in a column-wise manner using a codebook \mathcal{V} by means of

$$\mathcal{Q}_{1,k} : \mathbf{f}_k = \arg \max_{\mathbf{v}} |\mathbf{h}_k^H \mathbf{v}|^2 \quad \text{s.t.} \quad \mathbf{v} \in \mathcal{V} \setminus \bar{\mathcal{V}}, \forall k \in \mathcal{K}, \quad (3)$$

where $\bar{\nu}$ is formed by all the columns of ν that have already been assigned to some user. Initially, $\bar{\nu} = \emptyset$ and for each user the number of elements of $\bar{\nu}$ is increased by one.

Projection-based (PB): This method designs \mathbf{F} in an element-wise manner, given the set of phase shifts \mathcal{F} , via

$$\mathcal{Q}_{1,k} : \mathbf{f}_k = \underset{\mathbf{r}_k}{\operatorname{argmax}} \left| \mathbf{h}_k^H \mathbf{r}_k \right|^2 \quad \text{s.t.} \quad [\mathbf{r}_k]_n \in \mathcal{F}, n \in \mathcal{N}_1, \forall k \in \mathcal{K}. \quad (4)$$

First, the unconstrained version of $\mathcal{Q}_{1,k}$ is solved, whose solution collapses to the matched filter (i.e., a vector parallel to \mathbf{h}_k). Then, such vector is projected onto the set \mathcal{F} , thus yielding \mathbf{f}_k , i.e., $[\mathbf{f}_k]_n = \operatorname{argmax}_{\phi \in \mathcal{F}} \operatorname{Re} \{ \phi [\mathbf{h}_k]_n^* \}$.

Stage 2 (Rate-splitting and digital precoder design):

With the analog precoder \mathbf{F} designed, the problem that optimizes C_0 , $\{C_k\}_{k=1}^K$, $\{\mathbf{b}_k\}_{k=1}^K$, \mathbf{m} is given by

$$\mathcal{Q}_2 : \max_{C_0, C_k, \mathbf{b}_k, \mathbf{m}} \sum_{k \in \mathcal{K}} \mu_k \left(C_k + \log_2 \left(1 + \operatorname{SINR}_k^{(p)} \right) \right) \quad (5a)$$

$$\text{s.t.} \quad C_0 + \sum_{j \in \mathcal{K}} C_j \leq \log_2 \left(1 + \operatorname{SINR}_k^{(c)} \right), \forall k \in \mathcal{K}, \quad (5b)$$

$$(2c), (2d), (2e), \quad (5c)$$

where (2b) has been equivalently recast as (5b) since $\bar{R}^{(c)} \leq R_{\min}^{(c)}$. This nonconvex problem has been approached via the WMMSE method proposed in [2], [3], [5], which is shown to converge to a local optimum.

V. PROPOSED SOLUTION: FALCON

To solve \mathcal{Q}_2 , we propose FALCON, which does not require judicious selection of an initial feasible point. Our approach stems from exploiting level sets and the establishment of convex upper bounds that can be contracted iteratively. Thus, assuming that $\mathbf{g}_k = \mathbf{F}^H \mathbf{h}_k$, we equivalent recast \mathcal{Q}_2 as

$$\bar{\mathcal{Q}}_2 : \max_{C_0, C_k, \mathbf{b}_k, \mathbf{m}} \sum_{k \in \mathcal{K}} \mu_k \left(C_k + \log_2 (r_k) \right) \quad (6a)$$

$$\text{s.t.} \quad \left| \mathbf{g}_k^H \mathbf{b}_k \right|^2 \geq (r_k - 1) t_k, \forall k \in \mathcal{K}, \quad (6b)$$

$$\sum_{j \neq k} \left| \mathbf{g}_k^H \mathbf{b}_j \right|^2 + \sigma^2 \leq t_k, \forall k \in \mathcal{K}, \quad (6c)$$

$$C_0 + \sum_{j \in \mathcal{K}} C_j \leq \log_2 (z_k), \forall k \in \mathcal{K}, \quad (6d)$$

$$\left| \mathbf{g}_k^H \mathbf{m} \right|^2 \geq (z_k - 1) q_k, \forall k \in \mathcal{K}, \quad (6e)$$

$$\sum_{j \in \mathcal{K}} \left| \mathbf{g}_k^H \mathbf{b}_j \right|^2 + \sigma^2 \leq q_k, \forall k \in \mathcal{K}, \quad (6f)$$

$$r_k \geq 1, \forall k \in \mathcal{K}, \quad (6g)$$

$$z_k \geq 1, \forall k \in \mathcal{K}, \quad (6h)$$

$$(2c), (2d), (2e), \quad (6i)$$

In (6a), $1 + \operatorname{SINR}_k^{(p)}$ is lower-bounded by r_k whereas, in (6c), the denominator of $\operatorname{SINR}_k^{(p)}$ is upper-bounded by t_k . By combining these two relations, we obtain (6b). The constraints (6d), (6e) and (6f) are obtained in a similar manner.

Proposition 1: The formulations \mathcal{Q}_2 and $\bar{\mathcal{Q}}_2$ are equivalent.

Proof: We prove the equivalence by contradiction. Let $r_{k'}^*$, $t_{k'}^*$, $z_{k'}^*$, $q_{k'}^*$ denote the values of the variables for user k' at the optimum. Let us assume that at the optimum, constraint (6c) for user k' is inactive. Under this assumption, there must exist a strictly smaller $\hat{t}_{k'} < t_{k'}^*$ for which (6c) attains equality. This implies that there must also exist a strictly larger $\hat{r}_{k'} > r_{k'}^*$ that satisfies (6b), thus producing a larger objective (6a). This result contradicts the premise that we have obtained an optimal solution. Similar relations can be derived for (6d),

(6e), (6f), thus corroborating the equivalence of \mathcal{Q}_2 and $\bar{\mathcal{Q}}_2$. ■

$$\hat{\mathcal{Q}}_2 : \max_{C_0, C_k, \mathbf{B}_k, \mathbf{M}} \sum_{k \in \mathcal{K}} \mu_k \left(C_k + \log_2 (r_k) \right) \quad (7a)$$

$$\text{s.t.} \quad r_k t_k - t_k - \operatorname{Tr} (\mathbf{G}_k \mathbf{B}_k) \leq 0, \forall k \in \mathcal{K}, \quad (7b)$$

$$\sum_{j \neq k} \operatorname{Tr} (\mathbf{G}_k \mathbf{B}_j) + \sigma^2 - t_k \leq 0, \forall k \in \mathcal{K}, \quad (7c)$$

$$C_0 + \sum_{j \in \mathcal{K}} C_j \leq \log_2 (z_k), \forall k \in \mathcal{K}, \quad (7d)$$

$$z_k q_k - q_k - \operatorname{Tr} (\mathbf{G}_k \mathbf{M}) \leq 0, \forall k \in \mathcal{K}, \quad (7e)$$

$$\sum_{j \in \mathcal{K}} \operatorname{Tr} (\mathbf{G}_k \mathbf{B}_j) + \sigma^2 - q_k \leq 0, \forall k \in \mathcal{K}, \quad (7f)$$

$$\operatorname{Tr} (\mathbf{F}^H \mathbf{F} \mathbf{M}) + \sum_{k \in \mathcal{K}} \operatorname{Tr} (\mathbf{F}^H \mathbf{F} \mathbf{B}_k) \leq P_{\text{tx}}, \quad (7g)$$

$$\mathbf{B}_k \succeq \mathbf{0}, \forall k \in \mathcal{K}, \quad (7h)$$

$$\mathbf{M} \succeq \mathbf{0}, \quad (7i)$$

$$(2c), (2d), (6g), (6h), \quad (7j)$$

Via semidefinite programming, $\bar{\mathcal{Q}}_2$ is transformed into $\hat{\mathcal{Q}}_2$, where $\mathbf{G}_k = \mathbf{g}_k \mathbf{g}_k^H$, and the rank-one constraints on $\mathbf{B}_k = \mathbf{b}_k \mathbf{b}_k^H$, $\mathbf{M} = \mathbf{m} \mathbf{m}^H$ have been neglected. With the exception of constraints (7b), (7e), which contain quasi-concave functions of the form xy , the rest of expressions in $\hat{\mathcal{Q}}_2$ constitute a convex problem. In order to circumvent these constraints we resort to the inequality $\frac{\gamma}{2} x^2 + \frac{1}{2\gamma} y^2 \geq xy$, which arises from the arithmetic-geometric mean of γx^2 and $\frac{1}{\gamma} y^2$, for $\gamma > 0$ [7]. Upon applying this upper estimate to (7b), (7e), we obtain $\bar{\mathcal{Q}}_2$.

$$\bar{\mathcal{Q}}_2 : \max_{C_0, C_k, \mathbf{B}_k, \mathbf{M}} \sum_{k \in \mathcal{K}} \mu_k \left(C_k + \log_2 (r_k) \right) \quad (8a)$$

$$\text{s.t.} \quad \frac{\alpha_k}{2} r_k^2 + \frac{1}{2\alpha_k} t_k^2 - t_k - \operatorname{Tr} (\mathbf{G}_k \mathbf{B}_k) \leq 0, \forall k \in \mathcal{K}, \quad (8b)$$

$$\frac{\beta_k}{2} z_k^2 + \frac{1}{2\beta_k} q_k^2 - q_k - \operatorname{Tr} (\mathbf{G}_k \mathbf{M}) \leq 0, \forall k \in \mathcal{K}, \quad (8c)$$

$$\alpha_k > 0, \beta_k > 0, \forall k \in \mathcal{K}, \quad (8d)$$

$$(7c), (7d), (7f), (7g), (7h), (7i), (7j), \quad (8e)$$

Proposition 2: When $\gamma = y/x$, $\bar{\mathcal{Q}}_2$ and $\hat{\mathcal{Q}}_2$ are equivalent.

Proof: The geometric mean equates the arithmetic mean when the two constituents are equal, which occurs at $\gamma = y/x$. ■

Note that $\bar{\mathcal{Q}}_2$ is still nonconvex. However, we have removed the complicated constraints (7b), (7e) by incorporating auxiliary variables α_k and β_k . Notice that if α_k and β_k are fixed, $\bar{\mathcal{Q}}_2$ is convex. Therefore, we are in the position of tailoring an algorithm to solve $\bar{\mathcal{Q}}_2$. By harnessing *Proposition 2*, we propose Algorithm 1, wherein the upper estimates of $r_k t_k$ and $z_k q_k$ are contracted iteratively by updating α_k and β_k (i.e., lines 3, 4). Although Algorithm 1 solves $\bar{\mathcal{Q}}_2$, a solution to $\bar{\mathcal{Q}}_2$ may not be feasible to $\hat{\mathcal{Q}}_2$ or $\bar{\mathcal{Q}}_2$ due to omission of the rank-one constraints and the use of upper estimates. In the following, we clarify these aspects.

Proposition 3: The solutions to $\bar{\mathcal{Q}}_2^{(i)}$ have at most rank one.

Proof: Let $\bar{\mathcal{Q}}_2^{(i)}$ denote the i -th iteration of $\bar{\mathcal{Q}}_2$. Let the Lagrangian with respect to \mathbf{M} be defined as $\mathcal{L}_{\mathbf{M}} = \sum_{k \in \mathcal{K}} \xi_k \left(\frac{\beta_k}{2} z_k^2 + \frac{1}{2\beta_k} q_k^2 - q_k - \operatorname{Tr} (\mathbf{G}_k \mathbf{M}) \right) + \sum_{k \in \mathcal{K}} \pi_k (z_k q_k - q_k - \operatorname{Tr} (\mathbf{G}_k \mathbf{M})) + \epsilon (\operatorname{Tr} (\mathbf{F}^H \mathbf{F} \mathbf{M}) + \sum_{k \in \mathcal{K}} \operatorname{Tr} (\mathbf{F}^H \mathbf{F} \mathbf{B}_k) - P_{\text{tx}}) - \operatorname{Tr} (\mathbf{S} \mathbf{M})$, where $\xi_k \geq 0$, $\pi_k \geq 0$, $\epsilon \geq 0$, $\mathbf{S} \succcurlyeq \mathbf{0}$ are the dual variables. From the stationarity condition, we obtain $\mathbf{S} = \epsilon (\mathbf{F}^H \mathbf{F}) - \sum_{k \in \mathcal{K}} (\xi_k + \pi_k) \mathbf{G}_k \succcurlyeq \mathbf{0}$. Since $\mathbf{F}^H \mathbf{F}$ is positive definite, the equivalent relation $\epsilon \mathbf{I} - \sum_{k \in \mathcal{K}} (\xi_k + \pi_k) (\mathbf{F}^H \mathbf{F})^{-1} \mathbf{G}_k \succcurlyeq \mathbf{0}$ holds if $\epsilon \geq \lambda_{\max}(\mathbf{T})$, where λ_{\max} is the principal eigenvalue of $\mathbf{T} = \sum_{k \in \mathcal{K}} (\xi_k + \pi_k) (\mathbf{F}^H \mathbf{F})^{-1} \mathbf{G}_k \succcurlyeq \mathbf{0}$. When $\epsilon > \lambda_{\max}$, the matrix \mathbf{S} is positive definite and therefore $\operatorname{rank}(\mathbf{S}) = N_{\text{RF}}^{\text{tx}}$. Due to the complementary slackness condition, this implies that $\mathbf{M} = \mathbf{0}$. However, replacing $\mathbf{M} = \mathbf{0}$ in $\bar{\mathcal{Q}}_2^{(i)}$ yields $C_0 = 0$, which violates

(2c). Therefore this solution is not feasible. When $\epsilon = \lambda_{\max}$ then $\mathbf{S} \succ \mathbf{0}$. Consequently, $\text{rank}(\mathbf{S}) = N_{\text{RF}}^{\text{tx}} - 1$ and $\text{rank}(\mathbf{M}) = 1$, which satisfies the assertion. For the unicast precoders \mathbf{B}_k , similar relations can be derived. However, $\mathbf{B}_k = \mathbf{0}$ does not violate any constraint. In particular, $\mathbf{B}_k = \mathbf{0}$ can be optimal for a particular instance, specifically when the user weight μ_k is small compared to other weights. ■

Proposition 4: The sequence of objective function values produced by the update method in Algorithm 1 converges.

Proof: Let Ω_i denote the optimum of $\tilde{\mathcal{Q}}_2^{(i)}$. Also, let $f(\Omega_i)$ be the objective function of $\tilde{\mathcal{Q}}_2^{(i)}$ evaluated at the optimum Ω_i . Note that if we evaluate $f(\Omega_{i+1})$, all the constraints are still satisfied. This implies that an optimal solution to $\tilde{\mathcal{Q}}_2^{(i)}$ is feasible to $\tilde{\mathcal{Q}}_2^{(i+1)}$. Further, the update method (i.e., line 4) renders $f(\Omega_{i+1}) \geq f(\Omega_i)$, thus generating a monotonically non-decreasing sequence of objective function values. Moreover, since $\tilde{\mathcal{Q}}_2$ is limited by a power constraint, the non-decreasing sequence will be bounded and therefore guarantees convergence. ■

Proposition 5: $\tilde{\mathcal{Q}}_2$ satisfies the KKT conditions of \mathcal{Q}_2 .

Proof: A solution Ω_i to $\tilde{\mathcal{Q}}_2^{(i)}$ will always be feasible to $\tilde{\mathcal{Q}}_2$ as the inequalities of $\tilde{\mathcal{Q}}_2^{(i)}$ are tighter. Because a solution Ω_i with rank-one $\mathbf{M}^{(i)}$, $\mathbf{B}_k^{(i)}$, $\forall k \in \mathcal{K}$ can be found in $\tilde{\mathcal{Q}}_2^{(i)}$, Ω_i is also feasible to $\tilde{\mathcal{Q}}_2$ and \mathcal{Q}_2 . Invoking the results in Proposition 3.2 of [7], we state that the sequence of solutions $\{\Omega_i\}$ converges to a regular point Ω_i^* that is a KKT point of $\tilde{\mathcal{Q}}_2$ and \mathcal{Q}_2 . ■

Based on the propositions above, we show that via FALCON the feasible set of $\tilde{\mathcal{Q}}_2$ converges to the feasible set of \mathcal{Q}_2 . Further, by iteratively solving $\tilde{\mathcal{Q}}_2^{(i)}$ the solutions Ω_i converge to a local optimum of the nonconvex problem \mathcal{Q}_2 .

Algorithm 1: Rate-splitting and precoding via FALCON

Input: $\{\mathbf{h}_k\}_{k=1}^K$, $\{\mu_k\}_{k=1}^K$, C_0^{th} .
Output: \mathbf{F} , $\{\mathbf{b}_k\}_{k=1}^K$, \mathbf{m} , C_0 , $\{C_k\}_{k=1}^K$
Execute:
1: Design the analog precoder \mathbf{F} by solving $\mathcal{Q}_{1,k}$, $\forall k \in \mathcal{K}$.
2: Initialize $\alpha_k^{(i)} = 1$ and $\beta_k^{(i)} = 1$, $i = 0$, $\forall k \in \mathcal{K}$.
repeat
3: Solve $\tilde{\mathcal{Q}}_2^{(i)}$ employing $\alpha_k^{(i)}$ and $\beta_k^{(i)}$.
4: Update $\alpha_k^{(i+1)} = t_k^{(i)}/r_k^{(i)}$, $\beta_k^{(i+1)} = q_k^{(i)}/z_k^{(i)}$, $\forall k \in \mathcal{K}$.
5: Update $i = i + 1$.
until stopcriterion.

VI. SIMULATION RESULTS

In this section, we compare FALCON and WMMSE. In the scenarios evaluated in Section VI-A, Section VI-B, Section VI-C we employ the more versatile projection-based hybrid precoder whereas in Section VI-D we compare the two types of hybrid precoders. Throughout the simulations, we have considered $P_{\text{tx}} = 50$ dBm and $\sigma^2 = 30$ dBm as in [2]. In addition, for all scenarios involving different precoders and techniques, we have used the same stopping criterion (see Algorithm 1). Specifically, the techniques are executed for a maximum of $N_{\text{iter}} = 60$ iterations or until an increment of less than $\epsilon = 0.0001$ is attained (by the objective function).

Table I: Feasibility response of fully-digital precoders.

Case	Parameters configuration	WMMSE (%)															
		$P_m^{(0)} = 0.70P_{\text{tx}}$			$P_m^{(0)} = 0.80P_{\text{tx}}$			$P_m^{(0)} = 0.90P_{\text{tx}}$			$P_m^{(0)} = 0.95P_{\text{tx}}$			$P_m^{(0)} = 0.99P_{\text{tx}}$			
$[N_{\text{tx}}, K, C_0^{\text{th}}]$	(%)	MRT	ZF	SLNR	MRT	ZF	SLNR	MRT	ZF	SLNR	MRT	ZF	SLNR	MRT	ZF	SLNR	
A	[4, 2, 2.5]	100	38	55	54	63	63	63	75	77	73	83	83	78	84	83	80
B	[6, 3, 2.0]	100	36	49	68	51	63	70	70	80	77	81	83	81	87	87	83
C	[8, 4, 1.5]	96	53	67	86	69	73	89	80	85	93	83	85	93	91	92	94

Table II: Feasibility response of hybrid precoders.

Case	Parameters configuration	FALCON (%)	WMMSE (%)														
			$P_m^{(0)} = 0.70P_{\text{tx}}$			$P_m^{(0)} = 0.80P_{\text{tx}}$			$P_m^{(0)} = 0.90P_{\text{tx}}$			$P_m^{(0)} = 0.95P_{\text{tx}}$			$P_m^{(0)} = 0.99P_{\text{tx}}$		
$[N_{\text{tx}}, K, C_0^{\text{th}}]$	(%)	MRT	ZF	SLNR	MRT	ZF	SLNR	MRT	ZF	SLNR	MRT	ZF	SLNR	MRT	ZF	SLNR	
A	[4, 2, 2.5]	100	54	58	69	82	77	68	82	82	78	87	87	84	87	87	87
B	[6, 3, 2.0]	100	63	54	62	70	72	67	79	79	76	84	83	81	88	87	85
C	[8, 4, 1.5]	96	74	81	79	85	85	86	93	94	91	93	95	94	96	96	96

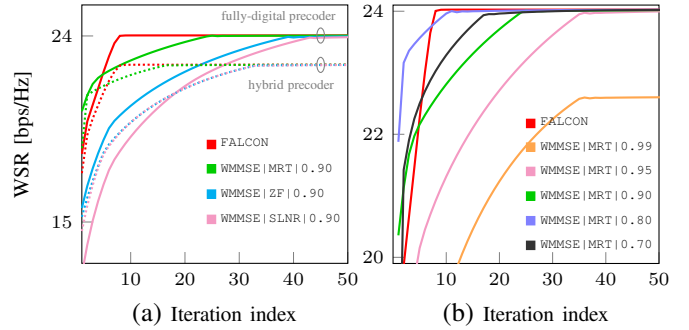


Figure 1: Convergence of FALCON and WMMSE.

A. Feasibility response

We evaluate the performance of FALCON and WMMSE with RS-NOUM, in terms of the feasible solutions count. We examine different configurations of $[N_{\text{tx}}, K, C_0^{\text{th}}]$ assuming equal weights $\mu_1 = \dots = \mu_K = 1$ with fully-digital and hybrid precoders. We employ the geometric Saleh-Valenzuela channel model [21]. Since WMMSE requires an initial feasible point, we assess three types of initialization methods. The initial multicast precoder $\mathbf{m}^{(0)}$ is obtained via singular value decomposition (SVD) of the aggregate channel [3], [19] whereas the initial unicast precoders $\mathbf{b}_k^{(0)}$ are the MRT, ZF or SLNR precoding vectors. The initial multicast and unicast powers (for the initial feasible point) are computed as $P_m^{(0)} = \|\mathbf{F}\mathbf{m}^{(0)}\|_2^2$ and $P_{u,k}^{(0)} = \|\mathbf{F}\mathbf{b}_k^{(0)}\|_2^2 = \frac{P_{\text{tx}} - P_m^{(0)}}{K}$, $\forall k \in \mathcal{K}$. We evaluate several values of $P^{(0)} = \{0.70P_{\text{tx}}, 0.80P_{\text{tx}}, 0.90P_{\text{tx}}, 0.95P_{\text{tx}}, 0.99P_{\text{tx}}\}$ with $L_{\text{tx}} = 16$ different phase shifts for the projection-based hybrid precoder. Table I and Table II show the results for the fully-digital and hybrid precoders. Note that FALCON is superior to WMMSE in delivering a larger number of feasible solutions without requiring complicated initialization. Throughout the different configurations, FALCON returns a feasible solution in at least 96% of the cases whereas the performance of WMMSE is inferior. In the WMMSE case, the same value of $P^{(0)}$ leads to different feasibility responses for distinct $[N_{\text{tx}}, K, C_0^{\text{th}}]$. In certain cases, the hybrid precoder attains more feasible solutions than the fully-digital precoder. This occurs due to the strong dependence of WMMSE on the initial feasible point, which is

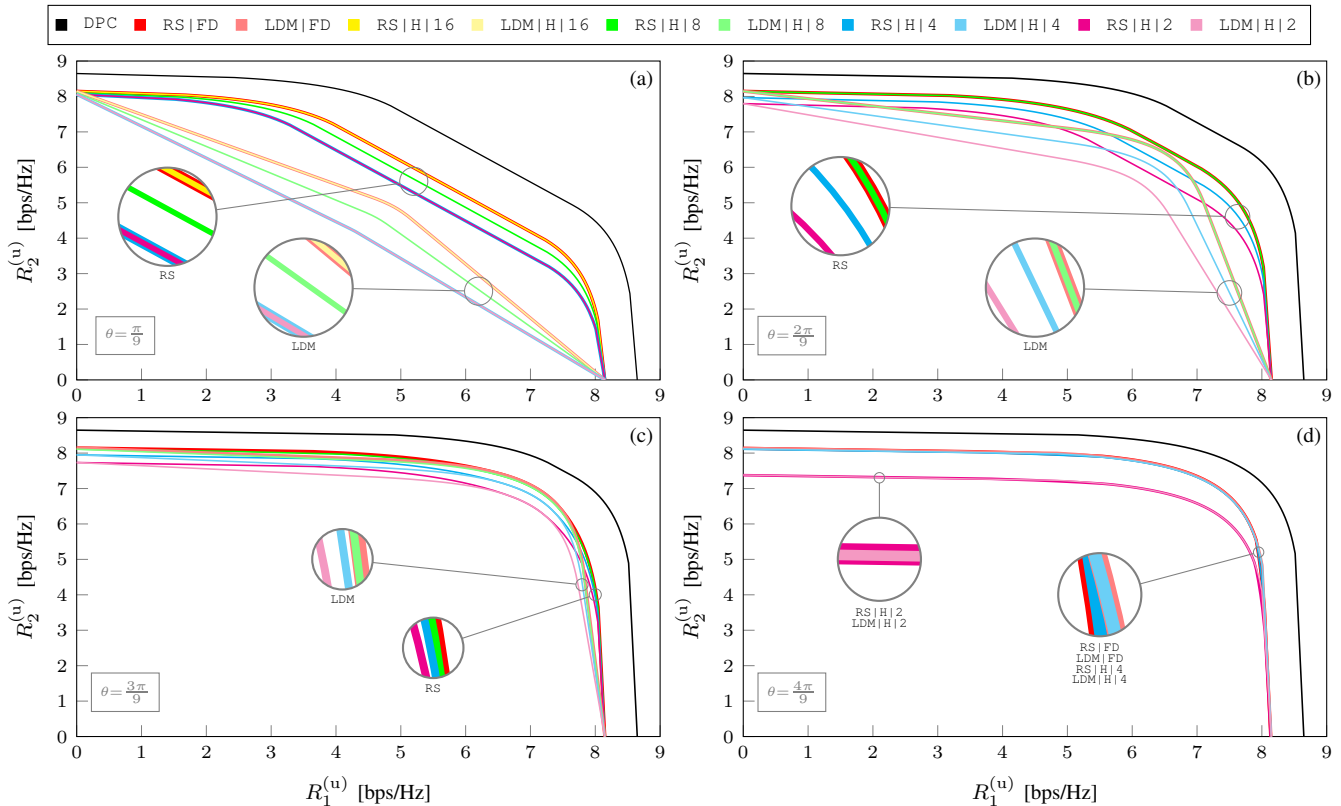


Figure 2: Two-user rate region for fully-digital (FD) and hybrid (H) precoders.

also influenced by the analog precoder F . Nevertheless, this outcome does not imply that both precoders provide the same rate value, as clarified in the next scenario.

B. Convergence

We compare the convergence of FALCON and WMMSE for a random realization of Case C in Table I, which is the most favorable scenario for WMMSE. Fig. 1a shows the evolution of the unicast rates when $P_m^{(0)} = 0.90P_{tx}$. We observe that FALCON converges 2 – 3 times faster than WMMSE for hybrid and fully-digital precoders. Since the performance of WMMSE relies on a initial point, in Fig. 1b we evaluate more cases for the fully-digital precoder using MRT (in [5] it is shown that MRT with SVD leads to faster convergence in high SNR regime as in this case). In Fig. 1b, although $P_m^{(0)} = 0.80P_{tx}$ produces faster convergence among other choices, it does not surpass FALCON, which only requires 8 iterations to attain convergence. Further, from Table I, using $P_m^{(0)} = 0.80P_{tx}$ only produces 69% of feasible solutions. Also, note that while $P_m^{(0)} = 0.99P_{tx}$ produces a feasible solution in 94% of the cases, this choice makes WMMSE converge to a less optimal point. Finding performant initial feasible points for WMMSE is impractical as either infeasibility certificates are returned or the convergence is impacted. In particular, we observe that WMMSE experiences the following trade-off: *large initial power allocation for $P_m^{(0)}$ leads to higher likelihood of producing feasible solutions but causes extremely slow convergence (optimality may even be affected) while small initial power allocations may produce*

faster convergence but increases the likelihood of resulting in infeasible solutions.

C. Two-user rate region

We evaluate the performance of RS-NOUM and LDM-NOUM using FALCON with fully-digital (FD) and projection-based hybrid (H) precoders considering the same settings as in [2], namely $K = 2$, $N_{tx} = 4$, $C_0^{th} = 0.5$ bps/Hz and channels $\mathbf{h}_1 = [1, 1, 1, 1]^H$, $\mathbf{h}_2 = [1, e^{j\theta}, e^{j2\theta}, e^{j3\theta}]^H$. For the hybrid precoder, we assume that $N_{tx}^{RF} = K = 2$ with four degrees of quantization, $L_{tx} = \{2, 4, 8, 16\}$. To solve the LDM case via FALCON, we enforce $C_k = 0, \forall k \in \mathcal{K}$. Fig. 2a shows the case when the channels are highly correlated ($\theta = \pi/9$). We observe that RS outperforms LDM due to its capability to manage interference, in particular in this challenging scenario. We also note that for RS and LDM, the hybrid precoder with $L_{tx} = 16$ (i.e., 4 bits) has the same performance as a fully-digital precoder. The performance when $L_{tx} = 2$ and $L_{tx} = 4$ is the same due to quantization that has produced the same analog precoder. Through Fig. 2b, Fig. 2c, Fig. 2d, the channel correlation among users is reduced by increasing θ . As expected, LDM approaches the performance of RS as interference becomes less detrimental. Interestingly, the phase resolution of the hybrid precoder becomes less relevant as the correlation between channels decreases. For instance, in Fig. 2d with $L_{tx} = 4$ (i.e., 2 bits) the hybrid and fully-digital precoders attain the same performance.

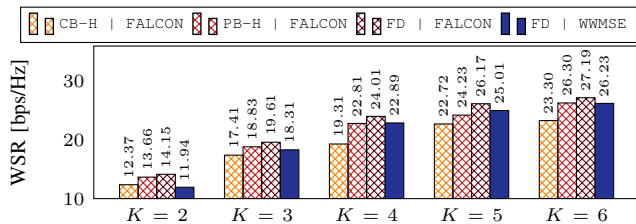


Figure 3: Performance comparison of hybrid precoders

Table III: Computational complexity per iteration

Description	Notation	Complexity
Weights of WMMSE with FD design	$\mathcal{C}_{\text{FD-WMMSE}}^{(w)}$	$\mathcal{O}(K^2 N_{\text{tx}})$
Precoders of WMMSE with FD design	$\mathcal{C}_{\text{FD-WMMSE}}^{(p)}$	$\mathcal{O}(K^{3.5} [N_{\text{tx}}]^{3.5})$
Weights of WMMSE with H design	$\mathcal{C}_{\text{H-WMMSE}}^{(w)}$	$\mathcal{O}(K^2 N_{\text{tx}}^{\text{RF}})$
Precoders of WMMSE with H design	$\mathcal{C}_{\text{H-WMMSE}}^{(p)}$	$\mathcal{O}(K^{3.5} [N_{\text{tx}}^{\text{RF}}]^{3.5})$
FALCON with FD design	$\mathcal{C}_{\text{FD-FALCON}}$	$\mathcal{O}(K^3 [N_{\text{tx}}]^6)$
FALCON with H design	$\mathcal{C}_{\text{H-FALCON}}$	$\mathcal{O}(K^3 [N_{\text{tx}}^{\text{RF}}]^6)$

D. Comparing hybrid precoder designs

We compare the performance of FALCON in RS-NOUM with the two hybrid precoder designs described in Section IV-B. In this scenario, we assume that $N_{\text{tx}} = 8$, $C_0^{\text{th}} = 1.5$ (as in Case C of Table I and Table II) for various number of users $K = \{2, 3, 4, 5, 6\}$. For the PB hybrid (PB-H) precoder we assume that $L_{\text{tx}} = 16$. For CB hybrid (CB-H) precoder, we form the codebook \mathcal{V} with 128 codewords, where N_{tx} codewords are mutually orthogonal obtained from the discrete Fourier matrix of size N_{tx} and 120 codewords pseudo-randomly generated. Fig. 3 shows that PB-H outperforms CB-H through all values of K . In addition, we include FALCON and WMMSE using fully-digital precoders. For WMMSE, we have assumed $P_m^{(0)} = 0.80P_{\text{tx}}$ because in Section VI-B we showed that this initial value does not affect performance substantially while allowing high convergence speed (although the feasibility ratio is conditioned).

E. Computational complexity

The computational complexity per iteration of WMMSE and FALCON with fully-digital (FD) or hybrid (H) precoders is shown in Table III. The complexity of designing the analog component \mathbf{F} has been considered negligible due to simple inner products involved. Since the complexity per iteration is not representative of the convergence behavior of a scheme, we show in Table IV the time required for convergence and the feasibility ratio. We evaluate FALCON and WMMSE using fully-digital precoders for the same scenario described in Section VI-D. We observe that while FALCON has higher computational complexity per iteration (see Table III), it converges up to 100% times faster (in terms of the execution time) and in addition, it returns more feasible solutions than WMMSE.

VII. CONCLUSION

We have investigated non-orthogonal unicast multicast transmissions by means of rate-splitting with fully-digital and hybrid precoders. We considered the weighted sum-rate

Table IV: Convergence time

Scheme	Number of users				
	$K = 6$	$K = 5$	$K = 4$	$K = 3$	$K = 2$
FALCON	93.6s 91%	40.1s 93%	33.8s 96%	31.7s 100%	37.5s 100%
WMMSE	116.9s 67%	75.9s 82%	66.3s 75%	45.1s 79%	31.4s 62%

maximization problem with a minimum multicast QoS requirement. We proposed FALCON based on sequential parametric optimization, which is shown to outperform WMMSE under a variety of scenarios. We showed that FALCON converges to local optimum of the nonconvex problem. Although FALCON has higher complexity per iteration than WMMSE, it converges faster within a few iterations and does not require an initial feasible point, which impacts performance. Further, FALCON is a viable option for designing hybrid precoders with rate-splitting since the complexity scales with the number of RF chains, which in general, is relatively small. In addition, for the two-user case, we noticed that a quantization scheme with 4 bits is sufficient for guaranteeing performance equal to that of a fully-digital precoder. Moreover, as the user channels become less correlated, the quantization granularity of the analog precoder is less relevant.

ACKNOWLEDGMENT

This research is funded by the Deutsche Forschungsgemeinschaft (DFG) within the B5G-Cell project in SFB 1053 MAKI, and the LOEWE initiative (Hesse, Germany) within the emergenCITY centre.

REFERENCES

- [1] J. Zhao, O. Simeone, D. Gunduz, and D. Gomez-Barquero, "Non-Orthogonal Unicast and Broadcast Transmission via Joint Beamforming and LDM in Cellular Networks," in *IEEE GLOBECOM*, December 2016, pp. 1–6.
- [2] Y. Mao, B. Clerckx, and V. O. K. Li, "Rate-Splitting for Multi-Antenna Non-Orthogonal Unicast and Multicast Transmission," in *IEEE SPAWC*, June 2018, pp. 1–5.
- [3] —, "Rate-Splitting for Multi-Antenna Non-Orthogonal Unicast and Multicast Transmission: Spectral and Energy Efficiency Analysis," *IEEE Transactions on Communications*, vol. 67, no. 12, pp. 8754–8770, December 2019.
- [4] H. Joudeh and B. Clerckx, "A Rate-Splitting Approach to Robust Multiuser MISO Transmission," in *IEEE ICASSP*, 2016, pp. 3436–3440.
- [5] —, "Sum-Rate Maximization for Linearly Precoded Downlink Multiuser MISO Systems With Partial CSIT: A Rate-Splitting Approach," *IEEE Transactions on Communications*, vol. 64, no. 11, pp. 4847–4861, November 2016.
- [6] S. S. Christensen, R. Agarwal, E. D. Carvalho, and J. M. Cioffi, "Weighted Sum-Rate Maximization Using Weighted MMSE for MIMO-BC Beamforming Design," *IEEE Transactions on Wireless Communications*, vol. 7, no. 12, pp. 4792–4799, December 2008.
- [7] A. Beck, A. Ben-Tal, and L. Tretuashvili, "A Sequential Parametric Convex Approximation Method with Applications to Nonconvex Truss Topology Design Problems," *Journal of Global Optimization*, vol. 47, no. 1, pp. 29–51, July 2010.
- [8] J. Zhao, D. Gündüz, O. Simeone, and D. Gómez-Barquero, "Non-Orthogonal Unicast and Broadcast Transmission via Joint Beamforming and LDM in Cellular Networks," *IEEE Transactions on Broadcasting*, pp. 1–13, June 2019.
- [9] Y. Liu, C. Lu, M. Tao, and J. Wu, "Joint Multicast and Unicast Beamforming for the MISO Downlink Interference Channel," in *IEEE SPAWC*, July 2017, pp. 1–5.
- [10] L. F. Abanto-Leon and G. H. Sim, "Fairness-Aware Hybrid Precoding for mmWave NOMA Unicast/Multicast Transmissions in Industrial IoTs," in *IEEE ICC*, June 2020.

- [11] Y. Li, M. Xia, and Y. Wu, "Energy-Efficient Precoding for Non-Orthogonal Multicast and Unicast Transmission via First-Order Algorithm," *IEEE Transactions on Wireless Communications*, vol. 18, no. 9, pp. 4590–4604, September 2019.
- [12] O. Tervo, L. Tran, S. Chatzinotas, M. Juntti, and B. Ottersten, "Energy-Efficient Joint Unicast and Multicast Beamforming with Multi-Antenna User Terminals," in *IEEE SPAWC*, July 2017, pp. 1–5.
- [13] E. Chen and M. Tao, "Backhaul-Constrained Joint Beamforming for Non-Orthogonal Multicast and Unicast Transmission," in *IEEE GLOBECOM*, December 2017, pp. 1–6.
- [14] E. Chen, M. Tao, and Y. Liu, "Joint Base Station Clustering and Beamforming for Non-Orthogonal Multicast and Unicast Transmission With Backhaul Constraints," *IEEE Transactions on Wireless Communications*, vol. 17, no. 9, pp. 6265–6279, September 2018.
- [15] L. F. Abanto-Leon, M. Hollick, and G. H. Sim, "BEAMWAVE: Cross-Layer Beamforming and Scheduling for Superimposed Transmissions in Industrial IoT mmWave Networks," in *Wireless Optimization*, October 2021.
- [16] O. Tervo, L. Tran, S. Chatzinotas, B. Ottersten, and M. Juntti, "Multigroup Multicast Beamforming and Antenna Selection with Rate-Splitting in Multicell Systems," in *IEEE SPAWC*, 2018, pp. 1–5.
- [17] H. Chen, D. Mi, Z. Chu, P. Xiao, and R. Tafazolli, "Rate-Splitting for Multigroup Multicast Beamforming in Multicarrier Systems," in *IEEE SPAWC*, 2018, pp. 1–5.
- [18] X. Su, L. Li, H. Yin, and P. Zhang, "Robust Power- and Rate-Splitting-Based Transceiver Design in K -User MISO SWIPT Interference Channel Under Imperfect CSIT," *IEEE Communications Letters*, vol. 23, no. 3, pp. 514–517, March 2019.
- [19] Y. Mao, B. Clerckx, and V. O. K. Li, "Rate-splitting Multiple Access for Downlink Communication Systems: Bridging, Generalizing, and Outperforming SDMA and NOMA," *EURASIP Journal on Wireless Communications and Networking*, vol. 1, no. 133, May 2018.
- [20] M. Dai and B. Clerckx, "Multiuser Millimeter Wave Beamforming Strategies With Quantized and Statistical CSIT," *IEEE Transactions on Wireless Communications*, vol. 16, no. 11, pp. 7025–7038, November 2017.
- [21] T. S. Rappaport, R. W. Heath, R. C. Daniels, and J. N. Murdock, *Millimeter Wave Wireless Communications*. New York: Pearson Education, 2015.